Josephson and noise scanning tunneling microscopy on conventional, unconventional and disordered superconductors

Chatzopoulos, D.

5

Noise doubling in Pb-I-Pb junctions

In this chapter we report on imaging the current noise with atomic resolution in a Pb-Pb junction using a Josephson scanning tunneling microscope. We measure the current noise as a function of applied bias to reveal the change from single electron tunneling above the superconducting gap energy to double electron charge transfer below the gap energy when Andreev processes become dominant. Our spatially resolved noise maps show that this doubling occurs homogeneously on the surface, including impurity locations, demonstrating that charge pairing is not influenced by disruptions in the superconductor smaller than the superconducting coherence length.

This chapter has been published in Physical Review B **100**, 104506 (2019).

5.1. Introduction

The coupling between two macroscopic superconducting electrodes through an insulating layer can lead to a dissipationless current called Josephson supercurrent. The critical current I_C is the maximal supercurrent that the junction can sustain; it is related to the individual superconducting order parameters in both electrodes, as well as their coupling [1]. In the zero-voltage limit, this supercurrent is carried by paired electrons (Cooper pairs), carrying twice the electron charge e. Applying a bias voltage V_B larger than twice the pair-breaking gap energy Δ, $eV_B > 2\Delta$, over the junction results in a normal current carried predominantly by quasiparticles with single electron charge (Fig. 5.1b). In the energy range below the gap edge, only so-called Andreev reflection processes can transport the quasiparticles across the junction by reflecting particles carrying opposite charge. These processes lead to effective charge transfer of multiple electron charges [2–4]. In the energy range $\Delta < eV_B < 2\Delta$, the dominant process is a single Andreev reflection leading to transfer of effectively double the electron charge, as illustrated in Fig. 5.1c.

One cannot tell from the time-averaged value of the current whether it is carried by multiple integers of charge, but this becomes apparent when measuring the fluctuations of the current, or in others words, the current noise [5–10]. In general, the noise originating from the flow of uncorrelated particles in a tunneling junction (shot noise) is a purely Poissonian process. The current noise power S_I is then proportional to the charge q and the current I of the carriers, $S = 2q|I|$ [5]. At lower bias voltages, when Andreev processes become relevant, the transferred charge in a Josephson junction can effectively double and therefore the noise is also expected to be two times the Poissonian value [11, 12]. Spectroscopic noise measurements in mesoscopic systems have revealed such noise signatures of multiple electron charge transport in superconducting junctions associated with Andreev processes [6–10], fractional charges in quantum hall systems [13, 14] and the vanishing of shot noise at atomic-scale point contacts [15–17].

Here, we perform such noise spectroscopy measurements spatially resolved with atomic resolution using a Josephson scanning tunneling microscope. We employ our recently developed noise scanning tunneling microscopy (NSTM) technique to spatially resolve the current and its time-resolved fluctuations simultaneously with atomic resolution [18]. We first demonstrate the current noise doubling from single to double charge transfer below the gap edge in a junction between a superconducting Pb tip and a Pb(111) sample. We then visualize this noise enhancement by spatially mapping the effective charge transfer over the sample surface. We show that it is homogeneous over the sample surface, also including impurity locations, demonstrating that the charge pairing is not influenced by disruptions smaller than the coherence length ($\xi \approx 80$ nm in Pb).

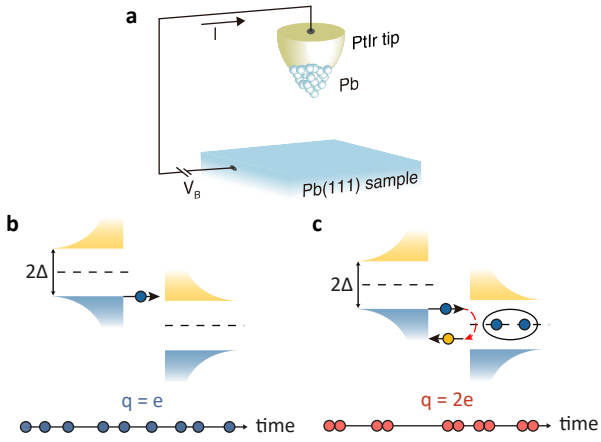

Figure 5.1: **Josephson scanning tunneling microscopy. a** Schematics of a Josephson scanning tunneling microscope. The SIS junction consists of a Pb-coated tip ($\Delta_{\mathrm{tip}} = 1.31$ meV) and a atomically flat Pb(111) surface ($\Delta_{\mathrm{sample}} = 1.35$ meV) separated by a thin vacuum barrier. **b** Normal current carried by quasiparticles transferring single electron charge. The characteristic density of states of both superconducting electrodes are shown, with filled/empty states denoted by blue/yellow separated by the pair-breaking gap $2\Delta_{\mathrm{tip/sample}}$. **c** Andreev reflection process. An electron transfers a Cooper-pair into the superconducting condensate by reflecting a hole in opposite direction, effectively transferring $2e$ charge.

5.2. Josephson scanning tunneling microscopy

A schematic of our setup is shown in Fig. 5.1, where a superconducting STM tip is brought in tunneling with a superconducting sample to form a superconductor-insulator-superconductor (SIS) junction. We create this junction in our modified low-temperature (2.2 K) Unisoku USM-1500 STM setup. First, the Pb(111) single crystal surface is cleaned by repetitive cycles of Ar^+ sputtering at 1kV with an Ar pressure of 5.0×10^{-5} mbar (background pressure $< 1.0 \times 10^{-10}$ mbar) and annealing. We then indent the mechanically grinded PtIr tip into the surface to decorate it with a superconducting cluster of Pb atoms until we obtain a SIS junction [19–21].

To demonstrate the high quality of the SIS junction in our setup, we display its distinct spectroscopic signatures for varying normal state resistance R_N in Fig. 5.2. The first signature is visible in the single particle channel, where quasiparticles with energies larger than the pair-breaking gap transfer the charge. The tunneling spectra in Fig. 5.2a show sharp coherence peaks, which are located at energies equal to the sum of both superconducting gaps of tip and sample $\Delta = \Delta_\mathrm{tip} + \Delta_\mathrm{sample} = 2.66$ meV. The clear U-shaped gap at 13.6 MΩ can be used as a benchmark for bulk-like superconducting properties of the tip and, also considering the low conductance, indicates that only a single transmission channel is present [22]. Due to the sharp density of states of the superconducting tip, the spectroscopic features are much sharper than one would expect from conventional thermal broadening [19]. We can fit these spectra with a modified phenomenological gap equation [23] to extract the effective electron temperature of 2.2 K, which is similar to the measured phonon temperature, as electron-phonon coupling is still rather efficient at these temperatures.

The next signature stems from Andreev processes that are visible at lower junction resistances. These lead to a sub-gap structure with humps in the differential conductance. Specifically, at energies below $2\Delta/n$, Andreev processes of order n become possible with relative probability τ^{n+1}, where τ is the transparency of the junction. A small hump, indicated by the black arrows in Fig. 5.2a and b, is visible in the differential conductance when the order of lowest allowed Andreev reflection process changes [2, 3].

The spectroscopic signatures related to the Josephson supercurrent in the junction are observed in the differential conductance at energies close to the Fermi level E_F: a peak that is enhanced with decreasing R_N, and small oscillations around the central peak (Fig. 5.2b). To understand these, we first survey the energy scales in our setup. The capacitive energy E_C and the thermal energy are larger than the Josephson energy E_J. Therefore, the environmental impedance becomes a relevant quantity, and thermal phase fluctuations across the junction govern the Josephson current, shifting the maximum current to a non-zero bias [24]. Close to the Fermi energy E_F we access the Cooper-pair channel associated with the coupling between the two superconducting condensates. The prominent peak at E_F in Fig. 5.2b, corresponding to the local maximum in the current in Fig. 5.2c, originates from the phase fluctuating Josephson current [21, 24]. Both the maximum Josephson current and the differential conductance at zero bias are proportional to the square of the intrinsic critical current of the Josephson junction [24]. The critical currents

we extract via the maximum value of the current in a small bias window around E_F show a linear relation with R_N and are well consistent with the Ambegaokar-Baratoff formula (Fig. 5.2d) [25]. We also note the small oscillating features in both the conductance and current spectra stretching far out to ~ 1 meV, originating from coupling of the junction with its dissipative electromagnetic environment, previously explained by a tip-induced antenna mode [21, 26].

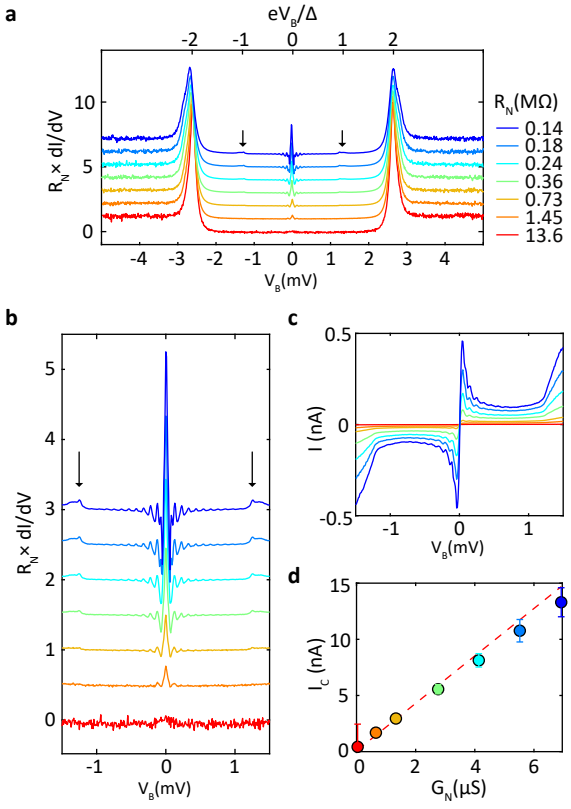

Figure 5.2: **Quasiparticle and Cooper pair tunneling signatures in a SIS Pb-Pb junction. a** Differential conductance spectra multiplied by the normal state resistance acquired for variable setup conditions. Sharp coherence peaks can be seen at $eV_B/\Delta = \pm 2$. The increasing conductance around $eV_B/\Delta = \pm 1$ (arrows) with variable normal state resistance indicates the presence of Andreev processes. **b** Zoom in at the low energy features in the differential conductance spectra. The prominent peak at the Fermi energy that rises with decreasing R_N is a signature of the Josephson supercurrent. **c** Current-voltage characteristics acquired simultaneously with the spectra shown in **b**. **d** Critical supercurrent of the junction (points) and its quantitative agreement with the Ambegaokar-Baratoff formula (red dashed line).

5.3. Scanning tunneling noise microscopy

We now want to come to the central part of this chapter, where we show the visualization of the doubling of the current noise in this scanning Josephson junction using NSTM. As we discussed in Chapter 2, the central challenge for measuring current noise in a conventional scanning tunneling microscope (STM) is that the temporal resolution is generally limited to only a few kHz, because the combination of the high impedance ($\sim$ GΩ) tunnel junction and capacitance of the interfacing cables (~ 100 pF) form an inherent low-pass filter. As a consequence, STM usually provides a static, time-averaged picture, lacking information about possible dynamical phenomena in the junction [27], especially when requiring atomic-resolution scanning.

Our noise measurement apparatus, described in Chapter 2 and in Ref. [18], builds upon earlier high-frequency STMs [28–30] but is based on a superconducting LC resonating circuit that is connected to the Josephson junction. Current fluctuations in the junction are converted into voltage fluctuations at resonance of the LC circuit, which are then amplified by the custom-built cryogenic amplifier [31] into a 50 Ω line.

5.4. Noise doubling due to Andreev reflections

We first measure the current noise as a function of energy at a single location. Fig. 5.3a shows the measured current noise power as function of bias, with the zero-current noise subtracted to remove the thermal noise component and input noise of the amplifier: $S_I(I) - S_I(0)$. The dashed lines indicate the theoretically calculated shot noise curves as described above, for effective charge e (blue) and $2e$ (red). At large bias voltage the experimental data follows the noise for single electron tunneling. However, the current noise clearly doubles from e to $2e$ at the coherence peak energy $eV_B/\Delta = \pm 2$. We obtain the effective charge q transferred through the junction by dividing the measured noise power by the full Poissonian noise $S = 2e|I| \coth \frac{qV}{2k_B T}$ (Fig. 5.3b). Note that, since we keep the junction resistance R_J constant, the transmission of the junction is changing when the bias voltage is reduced, leading to a correction of the effective q by $(1 - \tau_n)$ with $\tau_n \sim (G_0 R_J)^{-1/n}$ for small transparencies. The correction, applied to the data points in Fig. 5.3b is smaller than the scatter of our data points, due to the low transparency of our junction. The clear step in effective charge as a function of applied bias at the gap energy demonstrates that the tunneling current is now effectively carried by double charge quanta due to Andreev reflection processes. This is well consistent with theoretical descriptions [2–4, 11, 12] and experimental observations in mesoscopic devices, where Andreev reflections lead to enhanced noise in nanofabricated SIS junctions [9, 10] and short diffusive normal metal – superconductor contacts [6, 8], but has never been seen in a STM setup or at such low transparencies. In the present project, we use transparencies of $\tau \sim 10^{-3} - 10^{-4}$ leading to a single channel of transmission, whereas in mesoscopic devices usually multiple channels of $\tau \sim 10^{-1}$ are involved.

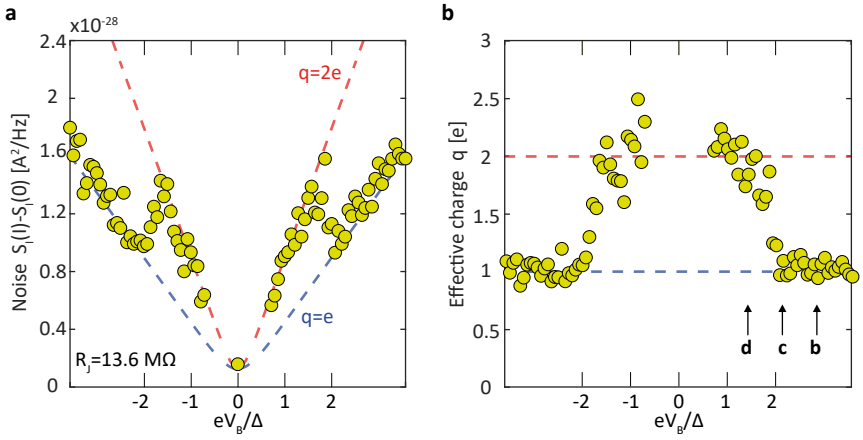

Figure 5.3: **Current noise as a function of bias voltage.** **a** Measured current noise for varying bias voltage acquired at a random location in Fig. 5.4a, maintaining a constant junction resistance $R_J = 13.6$ MΩ. The dashed lines represent the calculated values for effective charge equals e (blue) and $2e$ (red). **b** Effective charge transferred through the Josephson junction for varying bias. The data points represent $q = (S(I) - S(0))/2e|I|$, similar to the Fano factor. Dashed lines indicate $q = e$ and $q = 2e$ lines. The black arrows indicate the bias voltage of the spatially resolved noise maps of Fig. 5.4.

5.5. Spatially resolved noise doubling

Finally, we apply the spatial mapping capabilities of our NSTM setup to resolve this doubling of the noise over the sample surface with atomic-scale resolution. Figure 5.4a shows a topographic image of the Pb(111) surface in a 12,5 nm field of view, including a hexagonal shaped impurity previously identified as a sub-surface Ar nanocavity [32]. Next to locally reducing the scattering length, this nanocavity located beneath the surface also vertically and laterally confines charge carriers on a few nanometer length scale. We performed the noise-spectroscopy measurement in the same field of view by scanning the tip over the surface while simultaneously measuring the current noise. The spatially resolved noise maps at various bias voltages shown in Fig. 5.4b-d, exhibit a homogeneous contrast at energies above the pair-breaking gap energy, as is expected for transfer of uncorrelated particles. Below the superconducting gap energy we again observe homogeneous contrast, but now at an elevated value of the noise power around an effective charge equal to $2e$. While we observe a strong contrast in the topography, these spatially resolved noise maps show that the doubling occurs homogeneously over the surface, also on the location of the nanocavity. This demonstrates that disruptions in the superfluid, due to local confinement of the charge carriers or scattering on the nanocavity [32], on length scales smaller than the superconducting coherence length ($\xi \approx 80$ nm in Pb), do not influence the charge pairing, since the spatially resolved current noise is unaffected. This finding is in line with STM experiments showing that Andreev reflections are virtually unaffected by small diameter molecules [33].

5.6. Conclusions and outlook

In summary, we measured doubled shot noise caused by Andreev reflections in a Josephson scanning tunneling microscope using noise spectroscopy measurements. We spatially resolved this doubling with atomic-scale resolution on the surface of the conventional superconductor Pb(111). The ability to spatially resolve the charge dynamics with such precision opens new paths for investigating many-body correlation effects in quantum materials. Recently, it led to a novel understanding of cuprate high-temperature superconductors, where the discovery of charge trapping dynamics suggests a picture of copper-oxide planes separated by thin insulating layers within the three-dimensional superconducting state [34, 35]. Potentially, atomically resolved noise measurements will also reveal new insight in fluctuating stripe order [36] and pre-formed pairing in the pseudogap regime [37, 38], Kondo effects in heavy fermion systems [39], or signatures of Majorana modes in one-dimensional wires on a superconducting surface [40].

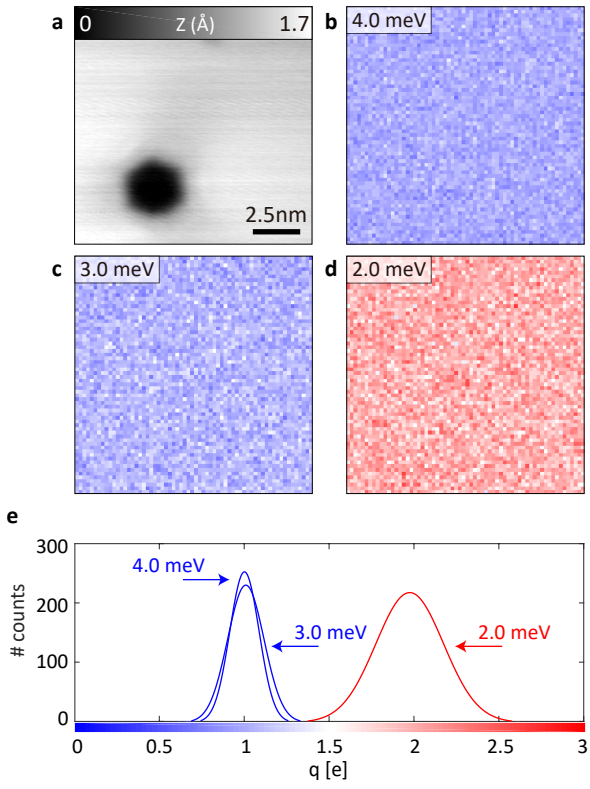

Figure 5.4: **Spatial mapping of the current noise.** **a** Topograph of 12,5 nm field of view on the Pb(111) surface, including a hexagonal shaped Ar nanocavity. **b-d** Spatial imaging of the effective charge for various bias voltages measured in feedback with a constant junction resistance $R_J = 13.6$ MΩ. The spatially resolved noise maps show homogeneous $q = e$ noise for $eV_B > 2\Delta$ (4.0 meV **b** and 3.0 meV **c**) and $q = 2e$ noise for $eV_B < 2\Delta$ (2.0 meV **d**). **e** Histograms showing the distribution of the effective charge for each spatial noise map.

References

[1] B. D. Josephson, *Possible new effects in superconductive tunnelling,* Phys. Lett. **1**, 251 (1963).

[2] G. E. Blonder, M. Tinkham, and T. M. Klapwijk, *Transition from metallic to tunneling regimes in superconducting microconstrictions: Excess current, charge imbalance, and supercurrent conversion,* Phys. Rev. B **25**, 4515 (1982).

[3] M. Octavio, M. Tinkham, G. E. Blonder, and T. M. Klapwijk, *Subharmonic energy-gap structure in superconducting constrictions,* Phys. Rev. B **27**, 6739 (1983).

[4] C. J. W. Beenakker, *Random-matrix theory of quantum transport,* Rev. Mod. Phys. **69**, 731 (1997).

[5] Y. M. Blanter and M. Büttiker, *Shot noise in mesoscopic conductors,* Phys. Rep. **336**, 1 (2000).

[6] X. Jehl, M. Sanquer, R. Calemczuk, and D. Mailly, *Detection of doubled shot noise in short normal-metal/superconductor junctions,* Nature **405**, 50 (2000).

[7] T. Hoss, C. Strunk, T. Nussbaumer, R. Huber, U. Staufer, and C. Schönenberger, *Multiple Andreev reflection and giant excess noise in diffusive superconductor/normal-metal/superconductor junctions,* Phys. Rev. B **62**, 4079 (2000).

[8] F. Lefloch, C. Hoffmann, M. Sanquer, and D. Quirion, *Doubled Full Shot Noise in Quantum Coherent Superconductor-Semiconductor Junctions,* Phys. Rev. Lett. **90**, 067002 (2003).

[9] Y. Ronen, Y. Cohen, J.-H. Kang, A. Haim, M.-T. Rieder, M. Heiblum, D. Mahalu, and H. Shtrikman, *Charge of a quasiparticle in a superconductor,* PNAS **113**, 1743 (2016).

[10] P. Dieleman, H. Bukkems, T. M. Klapwijk, M. Schicke, and K. Gundlach, *Observation of Andreev Reflection Enhanced Shot Noise,* Phys. Rev. Lett. **79**, 3486 (1997).

[11] M. J. M. de Jong and C. W. J. Beenakker, *Doubled shot noise in disordered normal-metal–superconductor junctions,* Phys. Rev. B **49**, 16070 (1994).

[12] J. C. Cuevas, A. Martín-Rodero, and A. L. Yeyati, *Shot noise and coherent multiple charge transfer in superconducting quantum point contacts,* Phys. Rev. Lett. **82**, 4086 (1999).

[13] R. De-Picciotto, M. Reznikov, M. Heiblum, V. Umansky, G. Bunin, and D. Mahalu, *Direct observation of a fractional charge,* Nature **389**, 162 (1997).

[14] L. Saminadayar, D. C. Glattli, Y. Jin, and B. Etienne, *Observation of the e/3 fractionally charged laughlin quasiparticle,* Phys. Rev. Lett. **79**, 2526 (1997).

[15] H. E. van den Brom and J. M. van Ruitenbeek, *Quantum suppression of shot noise in atom-size metallic contacts,* Phys. Rev. Lett. **82**, 1526 (1999).

[16] N. Agraıt, A. L. Yeyati, and J. M. Van Ruitenbeek, *Quantum properties of atomic-sized conductors,* Phys. Rep. **377**, 81 (2003).

[17] A. Burtzlaff, A. Weismann, M. Brandbyge, and R. Berndt, *Shot noise as a probe of spin-polarized transport through single atoms,* Phys. Rev. Lett. **114**, 016602 (2015).

[18] K. M. Bastiaans, T. Benschop, D. Chatzopoulos, D. Cho, Q. Dong, Y. Jin, and M. P. Allan, *Amplifier for scanning tunneling microscopy at MHz frequencies,* Rev. Sci. Instrum. **89**, 093709 (2018).

[19] M. Ruby, B. W. Heinrich, J. I. Pascual, and K. J. Franke, *Experimental demonstration of a two-band superconducting state for lead using scanning tunneling spectroscopy,* Phys. Rev. Lett. **114**, 157001 (2015).

[20] K. J. Franke, G. Schulze, and J. I. Pascual, *Competition of Superconducting Phenomena and Kondo Screening at the Nanoscale,* Science **332**, 940 (2011).

[21] M. T. Randeria, B. E. Feldman, I. K. Drozdov, and A. Yazdani, *Scanning Josephson spectroscopy on the atomic scale,* Phys. Rev. B **93**, 161115(R) (2016).

[22] E. Scheer, N. Agraït, J. C. Cuevas, A. L. Yeyati, B. Ludoph, A. Martín-Rodero, G. R. Bollinger, J. M. van Ruitenbeek, and C. Urbina, *The signature of chemical valence in the electrical conduction through a single-atom contact,* Nature **394**, 154 (1998).

[23] R. C. Dynes, V. Narayanamurti, and J. P. Garno, *Direct Measurement of Quasiparticle-Lifetime Broadening in a Strong-Coupled Superconductor,* Phys. Rev. Lett. **41**, 1509 (1978).

[24] G.-l. Ingold, H. Grabert, and U. Eberhardt, *Cooper-pair current through ultrasmall Josephson junctions,* Phys. Rev. B **50**, 395 (1994).

[25] V. Ambegaokar and A. Baratoff, *Tunneling between Superconductors,* Phys. Rev. Lett. **10**, 486 (1963).

[26] B. Jäck, M. Eltschka, M. Assig, A. Hardock, M. Etzkorn, and C. R. Ast, *A nanoscale gigahertz source realized with Josephson scanning tunneling microscopy,* Appl. Phys. Lett. **106**, 013109 (2015).

[27] C. J. Chen, *Introduction to Scanning Tunneling Microscopy Second Edition* (2008).

[28] H. Birk, M. J. M. de Jong, and C. Schönenberger, *Shot-noise suppression in the single-electron tunneling regime,* Phys. Rev. Lett. **75**, 1610 (1995).

[29] H. Birk, K. Oostveen, and C. Schönenberger, *Preamplifier for electric-current noise measurements at low temperatures,* Rev. Sci. Instrum. **67**, 2977 (1996).

[30] U. Kemiktarak, T. Ndukum, K. C. Schwab, and K. L. Ekinci, *Radio-frequency scanning tunnelling microscopy.* Nature **450**, 85 (2007).

[31] Q. Dong, Y. X. Liang, D. Ferry, A. Cavanna, U. Gennser, L. Couraud, and Y. Jin, *Ultra-low noise high electron mobility transistors for high-impedance and low-frequency deep cryogenic readout electronics,* Appl. Phys. Lett. **105**, 6 (2014).

[32] M. Müller, N. Néel, S. Crampin, and J. Kröger, *Lateral Electron Confinement with Open Boundaries: Quantum Well States above Nanocavities at Pb(111),* Phys. Rev. Lett. **117**, 136803 (2016).

[33] J. Brand, P. Ribeiro, N. Néel, S. Kirchner, and J. Kröger, *Impact of atomic-scale contact geometry on andreev reflection,* Phys. Rev. Lett. **118**, 107001 (2017).

[34] K. M. Bastiaans, D. Cho, T. Benschop, I. Battisti, Y. Huang, M. S. Golden, Q. Dong, Y. Jin, and M. P. Allan, *Charge trapping and super-Poissonian noise centres in a cuprate superconductor,* Nat. Phys. **14**, 1183 (2018).

[35] F. Massee, Y. K. Huang, M. S. Golden, and M. Aprili, *Noisy defects in the high-T_c superconductor $Bi_2Sr_2CaCu_2O_{8+x}$,* Nat. Commun. **10**, 544 (2019).

[36] E. W. Carlson, K. A. Dahmen, E. Fradkin, and S. A. Kivelson, *Hysteresis and noise from electronic nematicity in high-temperature superconductors,* Phys. Rev. Lett. **96**, 097003 (2006).

[37] P. A. Lee, *Amperean Pairing and the Pseudogap Phase of Cuprate Superconductors,* Phys. Rev. X **4**, 031017 (2014).

[38] B. Keimer, S. A. Kivelson, M. R. Norman, S. Uchida, and J. Zaanen, *From quantum matter to high-temperature superconductivity in copper oxides.* Nature **518**, 179 (2015).

[39] J. Figgins and D. K. Morr, *Differential conductance and quantum interference in Kondo systems,* Phys. Rev. Lett. **104**, 187202 (2010).

[40] S. Nadj-Perge, I. K. Drozdov, J. Li, H. Chen, S. Jeon, J. Seo, A. H. MacDonald, B. A. Bernevig, and A. Yazdani, *Topological matter. Observation of Majorana fermions in ferromagnetic atomic chains on a superconductor.* Science **346**, 602 (2014).